Donvil, Brecht; Muratore-Ginanneschi, Paolo; Pekola, Jukka P.

Hybrid master equation for calorimetric measurements

Published in:
Physical Review A

DOI:
10.1103/PhysRevA.99.042127

Published: 29/04/2019

Document Version
Publisher's PDF, also known as Version of record

Please cite the original version:
Donvil, B., Muratore-Ginanneschi, P., & Pekola, J. P. (2019). Hybrid master equation for calorimetric measurements. *Physical Review A*, *99*(4), 1-11. [042127]. https://doi.org/10.1103/PhysRevA.99.042127

Hybrid master equation for calorimetric measurements

Brecht Donvil[*] and Paolo Muratore-Ginanneschi[†]
Department of Mathematics and Statistics, University of Helsinki, P.O. Box 68, 00014 Helsinki, Finland

Jukka P. Pekola[‡]
Low Temperature Lab (OVLL), Aalto University School of Science, P.O. Box 13500, 00076 Aalto, Finland

(Received 30 November 2018; published 29 April 2019)

Ongoing experimental activity aims at calorimetric measurements of thermodynamic indicators of quantum integrated systems. We study a model of a driven qubit in contact with a finite-size thermal electron reservoir. The temperature of the reservoir changes due to energy exchanges with the qubit and an infinite-size phonon bath. Under the assumption of weak coupling and weak driving, we model the evolution of the qubit-electron temperature as a hybrid master equation for the density matrix of the qubit at different temperatures of the calorimeter. We compare the temperature evolution with an earlier treatment of the qubit-electron model, where the dynamics were modeled by a Floquet master equation under the assumption of drive intensity much larger than the qubit-electron coupling squared. We numerically and analytically investigate the predictions of the two mathematical models of dynamics in the weak-drive parametric region. We numerically determine the parametric regions where the two models of dynamics give distinct temperature predictions and those where their predictions match.

DOI: 10.1103/PhysRevA.99.042127

I. INTRODUCTION

The realization of efficient computing devices requires the understanding of the physical origins of heat production brought about by logical operations. Landauer's bound estimates that the minimum average energy dissipated while performing any irreversible logical operation, e.g., the erasure of one bit, is of the order of $O(k_BT)$ [1]. Recent experiments [2] showed the possibility to realize solid-state devices operating close to the Landauer bound. At the same time, a good understanding of the protocols to achieve the bound has been achieved for classical micro- and nanosystems [3,4]. Heat generation and control in a quantum integrated circuit still poses many challenges. As the system operates in contact with an environment, controlling thermodynamic indicators entails simultaneous monitoring of the system and the environment. Ultrasensitive radio-frequency calorimetric techniques afford a promising tool to monitor heat transfer in nanodevices down to subkelvin energy resolution [5,6].

With this motivation in mind, we derive theoretical predictions for the temperature statistics generated by the experimental setup for calorimetric measurements proposed by [7]. In essence, the setup is a nanoscale electric circuit, containing a superconducting qubit and a resistor element. The electrons in the resistor form a calorimeter, a finite-size environment of the qubit. The size of the resistor should be small enough such that temperature fluctuations due to energy exchanges between the qubit and calorimeter are detectable.

The proposal by [7] was previously modeled by [8] as a stochastic jump process for the state of the qubit and the temperature of the calorimeter. The authors of [9] introduced electron-phonon coupling to the model. This interaction leads to additional drift and diffusion terms in the evolution of the temperature of the electrons. Second, the authors supposed a strong periodic drive. Under this condition, they used the stochastic jump equation derived by [10], which is based on Floquet's theorem, to model the dynamics of the qubit. The stochastic jump process is an unravelling of the corresponding Floquet master equation, discussed in, for example, [11–14]. In the Floquet stochastic jump equation, the dynamics of the qubit are expressed in terms of solutions of the noninteracting periodically driven qubit. Modeling the dynamics as such is convenient to study the evolution of the electron temperature numerically and analytically. The authors of [9] expressed the qubit-calorimeter dynamics in terms of the Chapman-Kolmogorov-type master equation. In what follows, we refer to this equation as the Floquet master equation. One of the main results of [9] was to derive from the Floquet master equation a Fokker-Planck equation for the probability distribution of the electron temperature on long timescales, by eliminating the underlying qubit dynamics.

The disadvantage of using the Floquet stochastic equation is that it requires, in addition to the usual set of assumptions required for the Born-Markov approximation [15,16], that the strength of the drive be much larger than the qubit-calorimeter coupling squared [10]. This might not always be the physical reality in experiments. In the current paper, we aim to study the temperature behavior with a different model for the dynamics of the qubit. We use an unraveling [17] of the usual Lindblad equation where the drive is added as a perturbation to the nondissipative part. Besides the assumptions made for

[*]brecht.donvil@helsinki.fi
[†]paolo.muratore-ginanneschi@helsinki.fi
[‡]jukka.pekola@aalto.fi

the Born-Markov approximation, this approach requires the strength of the drive to be much smaller than the level spacing of the qubit.

One of our main results is the description of the qubit calorimeter as a hybrid master equation of the form of those introduced in [18,19]. A hybrid master equation describes the joint evolution of quantum and classical variables. In the present case these variables are the qubit wave function and the temperature of the calorimeter. The quantum discord related to temperature measurements of qubit-temperature states evolving according to the hybrid master equation is zero. This tells us that within our model by measuring the temperature, we cannot detect any quantumness [20].

If the qubit is driven long enough, the qubit calorimeter reaches a steady state: the electron temperature fluctuates around a stationary temperature T_S. On this timescale, it is possible to derive from the hybrid master equation an effective equation for the temperature evolution. The effective equation has the form of a time-autonomous Fokker-Planck equation. The qubit dynamics can be eliminated with the use of multitimescale perturbation theory. We numerically compare predictions of the hybrid and Floquet master equations. We identify the region of parameters in which the Floquet and weak drive dynamics give the same temperature predictions. We find for which values of the qubit-calorimeter coupling and drive strength both predict the same value for T_S. Experimentally, this a good indicator: measuring the average temperature is far easier than measuring the fluctuations.

The structure of the paper is as follows. In Sec. II, we briefly introduce the qubit-calorimeter model. We recap results by [8] to describe the evolution of the qubit calorimeter as a qubit-state-temperature process. In Sec. III, we describe the qubit-temperature process as a hybrid master equation for the qubit-temperature density operator. Section IV is devoted to deriving a Fokker-Planck equation for the temperature under the assumption of resonant driving of the qubit. On the hybrid master equation, we perform multitimescale perturbation theory in order to average out the qubit dynamics. In Sec. V, we numerically study the qubit-calorimeter model numerically and compare the results to those obtained from the Floquet modeling of the qubit dynamics. Finally, in Sec. VI, we briefly discuss the results.

II. QUBIT-CALORIMETER MODEL

We provide a short description of the qubit-calorimeter model as proposed by [7]. The setup consists of a driven qubit in contact with a finite-size electron bath on varying temperature T_e. The electron bath itself is in contact with an infinite-size thermal bath of phonons, on temperature T_p. It is essential for the experiment that the size of the electron bath is small enough such that fluctuations of the calorimeter temperature, due to energy exchange between the calorimeter and the qubit, can be detected. At the start of the experiment, both the qubit and calorimeter are in thermal equilibrium with the phonon bath. Subsequently, the qubit is driven out of equilibrium during which the electron temperature T_e is continuously monitored, in order to detect the aforementioned temperature fluctuations. We refer to [9] for further details.

Theoretically, the qubit-calorimeter phonon system is modeled by the Hamiltonian

$$H = H_q(t) + H_{qe} + H_e + H_{ep} + H_p. \tag{1}$$

The Hamiltonian of the qubit is

$$H_q(t) = \frac{\hbar\omega}{2}\sigma_z + \kappa\hbar\omega(e^{-i\omega_d t}\sigma_+ + e^{i\omega_d t}\sigma_-), \tag{2}$$

where σ_z denotes the canonical Pauli matrix and ω_d is the driving frequency. The interaction between the qubit and electrons is described by

$$H_{qe} = g\frac{\sqrt{8\pi}\epsilon_F}{3N}\sum_{k\neq l\in\mathbb{S}}(\sigma_+ + \sigma_-)a_k^\dagger a_l. \tag{3}$$

Here, σ_+ and σ_- are the creation and annihilation operator for the qubit and a_k, $a_k^\dagger$ for the electrons. The sum is restricted to an energy shell $\mathbb{S}$ close to the Fermi energy ϵ_F of the electrons. H_e and H_p are the free-electron and -phonon Hamiltonians and H_{ep} is the Fröhlich interaction term between them [21]. We will not explicitly study the electron-phonon interaction in this work. Earlier works [22–24] have shown that it induces a drift on the electron temperature towards the phonon temperature and additional noise.

In order to formulate an evolution equation for the qubit-calorimeter system, it is important to discuss the timescales involved in the model. The fastest timescale in the model is the relaxation time of the electrons to a thermal state [25], $\tau_{ee} \sim 1$ ns. The electron-phonon interaction takes place on a timescale $\tau_{ep} \sim 10^4$ ns [26] and the relaxation time of the qubit is typically up to $\tau_R \sim 10^5$ ns [27]. The large timescale separation $\tau_{ee} \ll \tau_R$ allows us to invoke the Markov approximation. Additionally, we assume that the characteristic timescale τ_{eq} of the qubit-calorimeter interaction satisfies $\tau_{eq} \ll \tau_{ep} \ll \tau_R$. Under this assumption, we can evaluate the qubit transition rates using the Fermi-Dirac distribution for the electron bath.

Under the above approximations, we express the qubit dynamics in terms of a stochastic Schrödinger equation, which consists of a continuous evolution interrupted by sudden jumps,

$$\begin{aligned} d\psi(t) &= \psi(t+dt) - \psi(t) \\ &= -iH_q(t)\psi(t)\,dt - \frac{1}{2}\{\Gamma_\downarrow[\sigma_+\sigma_- - \|\sigma_-\psi(t)\|^2]\psi(t) \\ &\quad + \Gamma_\uparrow[\sigma_-\sigma_+ - \|\sigma_+\psi(t)\|^2]\psi(t)\}\,dt \\ &\quad + \left[\frac{\sigma_-\psi(t)}{\|\sigma_-\psi(t)\|} - \psi(t)\right]dN_\downarrow + \left[\frac{\sigma_+\psi(t)}{\|\sigma_+\psi(t)\|} - \psi\right]dN_\uparrow, \end{aligned} \tag{4}$$

where $N_\downarrow$ and $N_\uparrow$ are Poisson counting processes. We estimate the temperature dependence of the calorimeter temperature on its energy with the Sommerfeld expansion; see, e.g., [28]. Under our assumptions, the energy E of the calorimeter only changes on timescales much larger than τ_{eq}. We find that

$$dT_e^2(t) = \frac{1}{N\gamma}\,dE(t), \tag{5}$$

where

$$\gamma = \frac{\pi^2 k_B^2}{4\epsilon_F}. \tag{6}$$

In our model, we have two contributions to the change in energy of the calorimeter,

$$dE(t) = dE_{eq}(t) + dE_{ep}(t). \tag{7}$$

The energy exchange due to interaction with the qubit is given by

$$dE_{eq}(t) = \hbar\omega(dN_\downarrow - dN_\uparrow). \tag{8}$$

The energy exchanged due to the electron-phonon interaction can be modeled by a drift and diffusion term [22–24],

$$dE_{ep}(t) = \Sigma V\left(T_p^5 - T_e^5\right)dt + \sqrt{10k_B\Sigma V}T_p^3\, dw(t), \tag{9}$$

where V is the volume of the calorimeter, Σ is a material constant, T_p is the phonon temperature, and $dw(t)$ is the increment of a Wiener process. The Poisson processes $N_\downarrow$ and $N_\uparrow$ are characterized by the conditional expectation values,

$$\mathsf{E}(dN_\uparrow|\psi, T) = \Gamma_\uparrow\|\sigma_+\psi\|^2\, dt, \tag{10}$$

$$\mathsf{E}(dN_\downarrow|\psi, T) = \Gamma_\downarrow\|\sigma_-\psi\|^2\, dt. \tag{11}$$

The decay rate is defined as

$$\Gamma_\downarrow = \begin{cases} \dfrac{g^2\omega\, e^{\hbar\omega/k_BT_e}}{e^{\hbar\omega/k_BT_e}-1} & \text{for} \quad T_e^2 > \frac{\hbar\omega}{N\gamma} \\ 1 & \text{for} \quad \frac{\hbar\omega}{N\gamma} \geqslant T_e^2 > 0, \end{cases} \tag{12a}$$

and the excitation rate equals

$$\Gamma_\uparrow = \begin{cases} \dfrac{g^2\omega}{e^{\hbar\omega/k_BT_e}-1} & \text{for} \quad T_e^2 > \frac{\hbar\omega}{N\gamma} \\ 0 & \text{for} \quad \frac{\hbar\omega}{N\gamma} \geqslant T_e^2 > 0. \end{cases} \tag{12b}$$

The excitation rate is set to zero for temperatures squared lower than $\hbar\omega/N\gamma$. In this case, an excitation of the qubit would lead to negative temperatures. While negative temperatures can be understood in terms of population inversion, in the present context we regard them as nonphysical: Equation (5) was derived using the Sommerfeld expansion for free electrons. In this context, a negative temperature implies an average energy of the electron bath lower than its ground-state energy. Concretely, it means that the electron bath does not have enough energy for an excitation of the qubit. We emphasize that in our numerical studies of the model, negative temperatures were never encountered.

From an experimental point of view, one is mainly interested in the evolution of the temperature. In the next sections, we show that on longer timescales of many periods of driving, it is possible to derive an effective evolution equation for the temperature.

III. HYBRID MASTER EQUATION

In order to eliminate the qubit process from the qubit-temperature evolution, it is convenient to first express the dynamics of the qubit-temperature in terms of a master equation. We define the process for the temperature squared $\xi(t) = T_e^2(t)$: Combining equations (5)–(9), $\xi(t)$ obeys the stochastic differential equation,

$$d\xi(t) = \frac{1}{N\gamma}\Big\{\hbar\omega(dN_\downarrow - dN_\uparrow) + \Sigma V\left[T_p^5 - \xi^{5/2}(t)\right]dt + \sqrt{10k_B\Sigma V}T_p^3\, dw_t\Big\}. \tag{13}$$

Let

$$P(\psi, \psi^*, X, t) = P[X \leqslant \xi(t) < X + dX \text{ and qubit in state } \psi] \tag{14}$$

be the probability for a qubit to be in a state ψ and the calorimeter to have temperature squared X at time t. In Appendix A, we derive a master equation for P and discuss the relative boundary conditions. For our purpose, however, it is more convenient to work with a different object than the full probability distribution. Let us first define the marginal temperature-squared distribution as

$$F(X, t) := \int D\psi D\psi^*\, \langle\psi|\mathbb{I}|\psi\rangle\, P(\psi, \psi^*, X, t). \tag{15}$$

Additionally, we introduce a notation for the expectation values of the canonical Pauli matrices at temperature-squared X,

$$\langle\sigma_i\rangle_X := \int D\psi D\psi^*\langle\psi|\sigma_i|\psi\rangle P(\psi, \psi^*, X, t), \tag{16}$$

with $i = z, y, z$. Using the above definitions, we define the qubit density operator at temperature-squared X as

$$\rho(X, t) := \tfrac{1}{2}[F(X, t)\mathbb{I} + \langle\vec{\sigma}\rangle_X \cdot \vec{\sigma}]. \tag{17}$$

The density operator $\rho(X, t)$ contains all information of the distribution $P(\psi, \psi^*, X, t)$ required to calculate moments of qubit observables depending on the electron temperature. In Appendix B, we show that $\rho(X, t)$ satisfies the master equation

$$\frac{d\rho}{dt}(X, t) = \frac{1}{N}\mathcal{L}_X\rho(X, t) + \rho(X, t) + M(\rho)(X, t), \tag{18}$$

with

$$\mathcal{L}_X\rho(X, t) = \mathcal{L}_X^{(1)}\rho(X, t) + \mathcal{L}_X^{(2)}\rho(X, t), \tag{19}$$

$$\mathcal{L}_X^{(1)}\rho(X, t) = -\frac{\Sigma V}{N\gamma}\partial_X\left[\left(T_p^5 - X^{5/2}\right)\rho(X, t)\right], \tag{20}$$

$$\mathcal{L}_X^{(2)}\rho(X, t) = \frac{\left(\sqrt{10\Sigma V k_B}T_p^3\right)^2}{2N^2\gamma^2}\partial_X^2\rho(X, t), \tag{21}$$

and

$$M(\rho)(X) = -\frac{i}{\hbar}[H(t), \rho(X)] + G_\downarrow\left(X - \frac{\hbar\omega}{N\gamma}\right)\sigma_-\rho\left(X - \frac{\hbar\omega}{N\gamma}\right)\sigma_+ + G_\uparrow\left(X + \frac{\hbar\omega}{N\gamma}\right)\sigma_+\rho\left(X + \frac{\hbar\omega}{N\gamma}\right)\sigma_- - \frac{1}{2}G_\downarrow(X)\{\sigma_+\sigma_-, \rho(X)\} - \frac{1}{2}G_\uparrow(X)\{\sigma_-\sigma_+, \rho(X)\}, \tag{22}$$

where we have defined

$$G_{\downarrow}(X) = \frac{g^2\omega\, e^{\hbar\omega/k_B\sqrt{X}}}{e^{\hbar\omega/k_B\sqrt{X}}-1}\theta\left(X-\frac{\hbar\omega}{N\gamma}\right)+\theta\left(\frac{\hbar\omega}{N\gamma}-X\right), \tag{23a}$$

$$G_{\uparrow}(X) = \frac{g^2\omega}{e^{\hbar\omega/k_B\sqrt{X}}-1}\theta\left(X-\frac{\hbar\omega}{N\gamma}\right), \tag{23b}$$

in accordance with the jump rates (12), to explicitly show the dependency on X.

Equation (18) is a hybrid master equation; it describes the joint evolution of the classical variable X and the quantum variable ψ. When the size of the calorimeter goes to infinity, $N \uparrow \infty$, qubit variables at different temperatures get decoupled and the above equation reduces to an ordinary Lindblad equation for a qubit interacting with a thermal environment.

In Appendix B, we show that our equation can be identified with a hybrid master equation of the form discussed in [18,19]. From one of the results in [18], we deduce that when only the temperature is measured, the quantum discord of a state $\rho(X)$ is zero. Quantum discord is defined as the difference between two classically equivalent expressions for mutual information [20]. It is an indicator for the quantumness of the correlations obtained from measuring the temperature. Equation (18) is not of the form of a classical Pauli master equation, as is the case for the Floquet approach [9]. Nevertheless, from the quantum discord being zero, we can conclude that by measuring the temperature, we cannot detect quantum effects.

IV. EFFECTIVE TEMPERATURE PROCESS

Let us now assume the existence of a separation of timescales in the model, namely, that temperature of the calorimeter equilibrates much slower than the qubit does. Concretely, we will expand the dynamics under the limit of an infinite-size calorimeter, and work a timescale on which the temperature evolves and the qubit has already relaxed. The expansion parameter is the inverse of the amount of electrons N in the calorimeter,

$$\varepsilon = \frac{1}{N}. \tag{24}$$

The qubit dynamics take place on the timescale set by t; for the temperature dynamics, we introduce the second time,

$$\tau = \epsilon t. \tag{25}$$

When we write the dependence of the density operator ρ on the two scales,

$$\rho(X,t) = \tilde{\rho}(X,t,\tau), \tag{26}$$

the time derivative becomes

$$\frac{d\rho}{dt}(X,t) = \partial_t\tilde{\rho}(X,t,\tau)+\epsilon\partial_\tau\tilde{\rho}(X,t,\tau). \tag{27}$$

To perform the perturbative expansion, we assume that the process has already relaxed on the shortest timescale. We consider the density operator

$$\bar{\rho}(X,\tau) = \lim_{t\uparrow+\infty}\tilde{\rho}(X,t,\tau), \tag{28}$$

which has already relaxed on the shortest timescale. It is convenient to write the matrix elements of $\rho(X,\tau)$,

$$\bar{\rho}(X,\tau) = \begin{pmatrix} P_1(X,\tau) & P_3(X,\tau) \\ P_4(X,\tau) & P_2(X,\tau)\end{pmatrix}, \tag{29}$$

into a vector $\vec{P}(X,\tau)$. By the definition of $\rho(X,t)$ (17), we can see that the off-diagonal elements

$$P_3(X,\tau) = \tfrac{1}{2}\langle\sigma_x - i\sigma_y\rangle_X = \langle\sigma_-\rangle_X, \tag{30a}$$

$$P_4(X,\tau) = \tfrac{1}{2}\langle\sigma_x + i\sigma_y\rangle_X = \langle\sigma_+\rangle_X \tag{30b}$$

are each other's adjoint. Expanding Eq. (18) in terms of ε and using Eq. (27), we get into

$$\varepsilon\frac{d\vec{P}(X,\tau)}{dt} = \varepsilon\mathcal{L}^{(1)}\vec{P}(X,\tau)+\varepsilon^2\mathcal{L}^{(2)}\vec{P}(X,\tau) + M^{(0)}(\vec{P})(X,\tau)+\sum_{n=1}\frac{\varepsilon^n}{n!}\partial_X^n[M^{(n)}(\vec{P})(X,\tau)], \tag{31}$$

with

$$M^{(0)} = \begin{pmatrix} -G_{\downarrow}(X) & G_{\uparrow}(X) & i\lambda & -i\lambda \\ G_{\downarrow}(X) & -G_{\uparrow}(X) & -i\lambda & i\lambda \\ i\lambda & -i\lambda & -G(X)/2 & 0 \\ -i\lambda & i\lambda & 0 & -G(X)/2\end{pmatrix}. \tag{32}$$

The sum of the rates is defined as

$$G(X) = G_{\downarrow}(X)+G_{\uparrow}(X) \tag{33}$$

and the higher orders in the expansion of M are

$$M^{(n)} = \left(\frac{\hbar\omega}{\gamma}\right)^n\begin{pmatrix} 0 & G_{\uparrow}(X) & 0 & 0 \\ (-1)^n G_{\downarrow}(X) & 0 & 0 & 0 \\ 0 & 0 & 0 & 0 \\ 0 & 0 & 0 & 0\end{pmatrix}. \tag{34}$$

Note that the matrix M^0 corresponds to the Lindblad equation in the infinite calorimeter limit.

In Appendix C, we solve Eq. (31) at different orders in ε using a Hilbert expansion [29] of the probability distribution,

$$\vec{P}(X,t) = \sum_{n=0}^{+\infty}\epsilon^n\vec{P}^n(X,t). \tag{35}$$

The marginal temperature distribution is obtained by taking the trace of $\bar{\rho}$ [see Eq. (17)], which corresponds to summing the first two components of $\vec{P}$ (29):

$$F(X,\tau) = P_1(X,\tau)+P_2(X,\tau) = \sum_{n=0}^{\infty}\varepsilon^n\left[P_1^{(n)}(X,\tau)+P_2^{(n)}(X,\tau)\right] = \sum_{n=0}^{\infty}\varepsilon^n F^{(n)}(X,\tau). \tag{36}$$

The result of Appendix C is an effective equation for $F(X,\tau) = F^{(0)}(X,\tau) + \varepsilon F^{(1)}(X,\tau)$ up to second order in ε for resonant driving,

$$\partial_\tau F(X,\tau) = -\partial_X \left\{ \left[\frac{\Sigma V}{N\gamma}\left(T_p^5 - X^{5/2}\right) + \frac{1}{N} j^{(1)}(X) + \frac{1}{N^2} j^{(2)}(X) \right] F(X,\tau) \right\} + \partial_X^2 \left\{ \left[\frac{\left(\sqrt{10\Sigma V k_B} T_p^3\right)^2}{2N^2\gamma^2} + \frac{1}{N^2}\Delta^{(1)}(X) + \frac{1}{N^2}\Delta^{(2)}(X) \right] F(X,\tau) \right\}, \tag{37}$$

where we have defined the corrections to the drift as

$$j^{(1)}(X) = -\langle v_1, M^{(1)} Q\rangle, \tag{38}$$

$$j^{(2)}(X) = -\left\langle v_1 | \partial_X \left(\frac{1}{\lambda_3 \langle v_3|w_3\rangle} |M^{(1)} w_3\rangle\langle v_3| \right) M^{(1)} Q \right\rangle - \left\langle v_1 \partial_X \left(\frac{1}{\lambda_4\langle v_4|w_4\rangle} |M^{(1)} w_4\rangle\langle v_4| \right), M^{(1)} Q \right\rangle - \frac{1}{\lambda_4\langle v_4|w_4\rangle}\langle v_1|M^{(1)}w_4\rangle\langle v_4|(\mathcal{L}^{(1)})^\dagger Q\rangle - \frac{1}{\lambda_3\langle v_3|w_3\rangle}\langle v_1|M^{(1)}w_3\rangle\langle v_3|(\mathcal{L}^{(1)})^\dagger Q\rangle. \tag{39}$$

And the corrections to the diffusion coefficient are

$$\Delta^{(1)}(X) = \tfrac{1}{2}\langle v_1|M^{(2)}Q\rangle, \tag{40}$$

$$\Delta^{(2)}(X) = -\frac{1}{\lambda_4\langle v_4|w_4\rangle}\langle v_1|M^{(1)}w_4\rangle\langle v_4|M^{(1)}Q\rangle - \frac{1}{\lambda_3\langle v_3|w_3\rangle}\langle v_1|M^{(1)}w_3\rangle\langle v_3|M^{(1)}Q\rangle. \tag{41}$$

The effective equation for the evolution of the temperature distribution (37) has the form of a time-autonomous Fokker-Planck equation.

The stationary temperature T_S is defined as the square root of X_S, for which the drift coefficient is zero. The lowest-order correction to the drift $j^{(1)}(X)$ explicitly allows us to estimate the dependence of the stationary temperature T_S on the qubit-calorimeter coupling g and the driving strength κ,

$$j^{(1)}(X) = \frac{\hbar\omega^2 g^2 4\kappa^2}{g^4 \coth^2\left(\frac{\hbar\omega}{2k_B\sqrt{X}}\right) + 8\kappa^2}. \tag{42}$$

For large $\hbar\omega/(2k_B\sqrt{X})$, i.e., for small X, $\coth[\hbar\omega/(2k_B\sqrt{X})] \approx 1$. Under this approximation, we find that

$$T_S \approx \left(T_p^5 + \frac{1}{\Sigma V}\frac{\hbar\omega^2 g^2 4\kappa^2}{g^4 + 8\kappa^2} \right)^{1/5}. \tag{43}$$

Using the Floquet approach, the g dependence of T_S was found to be [9]

$$T_S \approx \left(T_p^5 + g^2 \frac{O(\hbar\omega^2)}{\Sigma V} \right)^{1/5}, \tag{44}$$

where the weak dependence on the strength of the drive κ is hidden in $O(\hbar\omega^2)$. For $g^2 \ll \kappa$, i.e., the range in which the Floquet stochastic process is valid, both expressions show the same g dependence.

V. SIMULATIONS

We aim to compare temperature predictions by the weak-drive modeling of the qubit dynamics to those of the Floquet modeling studied in [9]. For the numerical integration of the dynamics, we take the similar parameters as [9]. The level spacing of the qubit is $\hbar\omega = 0.5 k_B \times 1\,\mathrm{K}$, the volume of the calorimeter is $V = 10^{-21}\ \mathrm{m}^3$, $\Sigma = 2\times 10^{-9}\,\mathrm{W\,K^{-5}\,m^{-3}}$, and $\gamma = 1500 k_B/(1\,\mathrm{K})$. The strength of the drive κ and the qubit-calorimeter coupling g will be varied during the numerics.

The experimental protocol described by [7] is as follows: Initially the qubit and calorimeter are in thermal equilibrium with an infinite-size phonon bath, i.e., the substrate on which the circuit is mounted. Then the qubit is driven out of equilibrium while keeping track of the energy exchanges between qubit and calorimeter by continuously measuring the temperature of the latter. As such, in the beginning of our numerical simulations of the experiment, the initial state of the qubit is drawn from a thermal distribution with phonon temperature T_p.

In order to numerically integrate the dynamics of the qubit-calorimeter system, time is discretized into steps of the size $dt = (1000\omega_q)^{-1}$. The qubit state $\psi(t)$ and the electron temperature $T_e(t)$ are then updated from time t to $t + dt$ in three steps: (1) the jump rates $\Gamma_{\uparrow/\downarrow}$ are calculated from $\psi(t)$ and $T_e(t)$; (2) a random-number generator decides whether the system makes a jump; and (3) $\psi(t + dt)$ and $T_e(t + dt)$ are calculated using Eqs. (4) and (13).

Figure 1 shows the temperature distribution of the calorimeter after a driving duration of 10 periods of the qubit $T = 2\pi/\omega$. It is obtained from 10^4 repetitions of numerically integrating Eqs. (4) and (13). For low coupling strength g^2, the (red) line from the Floquet modeling overlaps with the (blue) histogram weak-drive modeling. When g^2 is increased, the temperature distribution is shifted to the right, indicating that the assumptions required for the Floquet modeling of the qubit dynamics are broken. In this regime, the latter overestimates the power exerted by the qubit. The explanation of the overestimate of the power resides in the assumption $\kappa \gg g^2$ needed to derive the Floquet jump equation.

The mean and standard deviation of the temperature distribution as a function of the ratio of the driving and qubit frequency ω_d/ω after driving a duration of 10 periods of

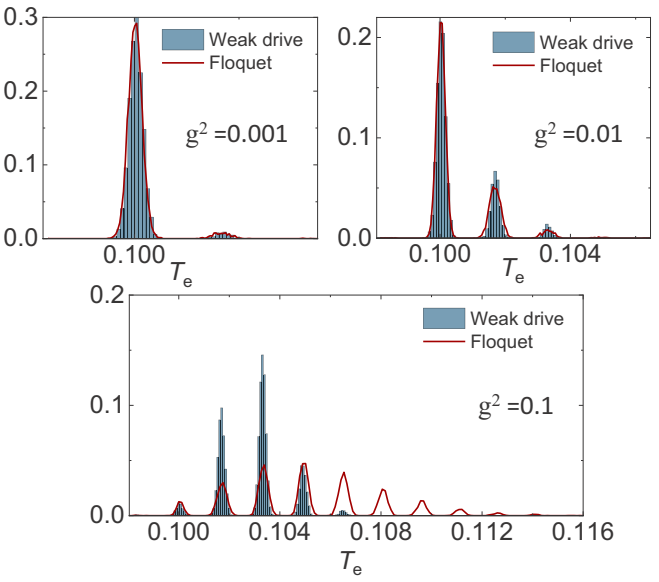

FIG. 1. Distribution of the electron temperature T_e after a driving duration of $10 \times 2\pi/\omega$ for different values of the qubit calorimeter g and $\kappa = 0.05$. The full (red) line is the distribution obtained from numerically integrating the qubit-temperature evolution with Floquet dynamics for the qubit, and the (blue) histogram comes from the weak-drive dynamics (4) and (13), both from 10^4 repetitions. The physical parameters used in the numerical integration are $\hbar\omega = 0.5k_B \times 1\,\mathrm{K}$, $V = 10^{-21}\,\mathrm{m}^3$, $\Sigma = 2 \times 10^{-9}\,\mathrm{W\,K^{-5}\,m^{-3}}$, and $\gamma = 1500k_B/(1\,\mathrm{K})$.

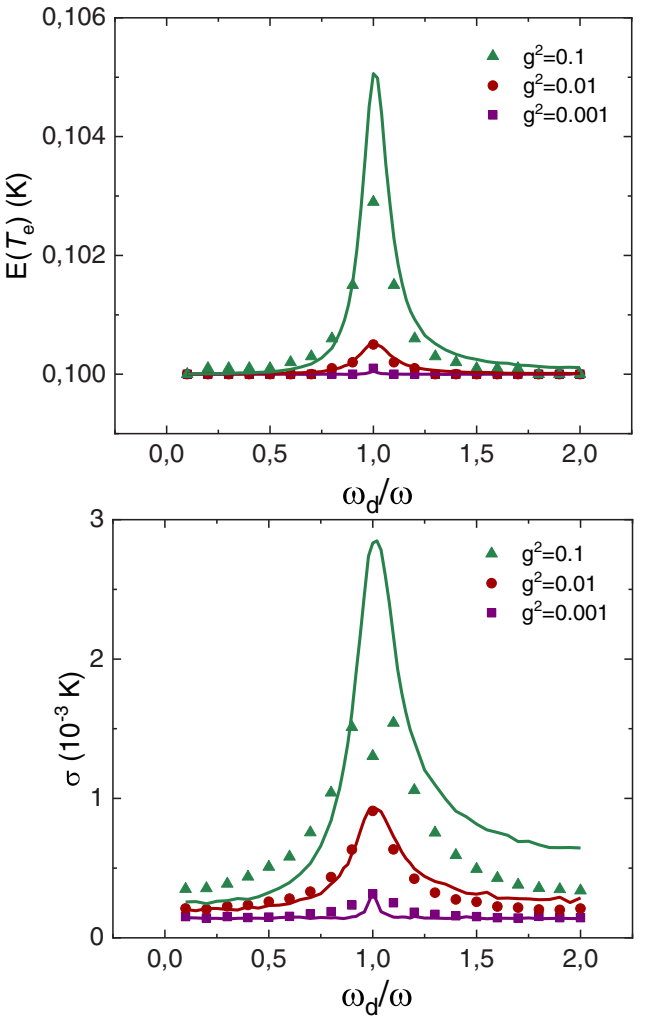

FIG. 2. Mean (top) and standard deviation (bottom) of the temperature distribution after driving a duration of $10 \times 2\pi/\omega$ (see Fig. 1) as a function of the ratio of the driving and qubit frequency ω_d/ω for different values of the qubit-calorimeter coupling g. The stars are obtained from numerically integrating the qubit-temperature jump process with the weak-drive qubit dynamics (4) and (13), and the full lines are from numerically integrating with the Floquet modeling of the qubit dynamics [9]. The parameters used for the simulations are in the caption of Fig. 1.

the qubit are shown in Fig. 2. The full lines are obtained from the Floquet modeling, while the points are from the numerics of the weak drive. Again we see that for low enough coupling g^2, the predictions from both modelings correspond well.

Figure 3(a) shows the mean temperature of the calorimeter, after it has reached a steady state. The mean is an estimate for the stationary temperature T_S of the effective Fokker-Planck equation (37). The estimate of the stationary temperature is shown as a function of the driving strength κ for different qubit-calorimeter coupling g^2 values. The value of T_S predicted by the weak-drive modeling of the qubit dynamics asymptotically reaches the Floquet-modeling prediction. The parametric region that we consider, $\kappa \sim O(10^{-2})$ and $g^2 \sim O(10^{-1})$, is in the the range of weak driving. For large enough driving strength κ compared to g^2, both approaches predict the same value for T_S. This indicates that the assumption $\kappa \gg g^2$ required for the Floquet modeling is met. By using T_S as an indicator, we can estimate the parametric region of validity for the Floquet modeling of the qubit dynamics. Figure 3(b) shows that estimated region. The region where the weak-drive dynamics estimate for T_S plus one standard deviation obtained from numerics exceeds the predicted value by the Floquet modeling is colored. This corresponds to the points in Fig. 3 where the error bars on the dots exceed the striped asymptotes. The slope between the two regions is 0.454 ± 0.013, which means that κ has to be about twice as large as g^2 for the Floquet modeling to hold. The experiment proposed by [7] has the aim to measure the temperature of the bath. By measuring the steady-state temperature at different levels of driving strength, it is possible to detect in which regime the Floquet approach holds for the experimental setup.

Figure 4 shows the temperature steady-state distribution obtained from the numerics. It is compared to the steady-state distribution of the Fokker-Planck equation (37) and the Fokker-Planck equation from the Floquet modeling [9]. The distributions in the right figure correspond well; the values of κ and g^2 are inside the green region in Fig. 3(b).

VI. CONCLUSION

The evolution of the state and the qubit and temperature of the calorimeter can be formulated in terms of a hybrid master

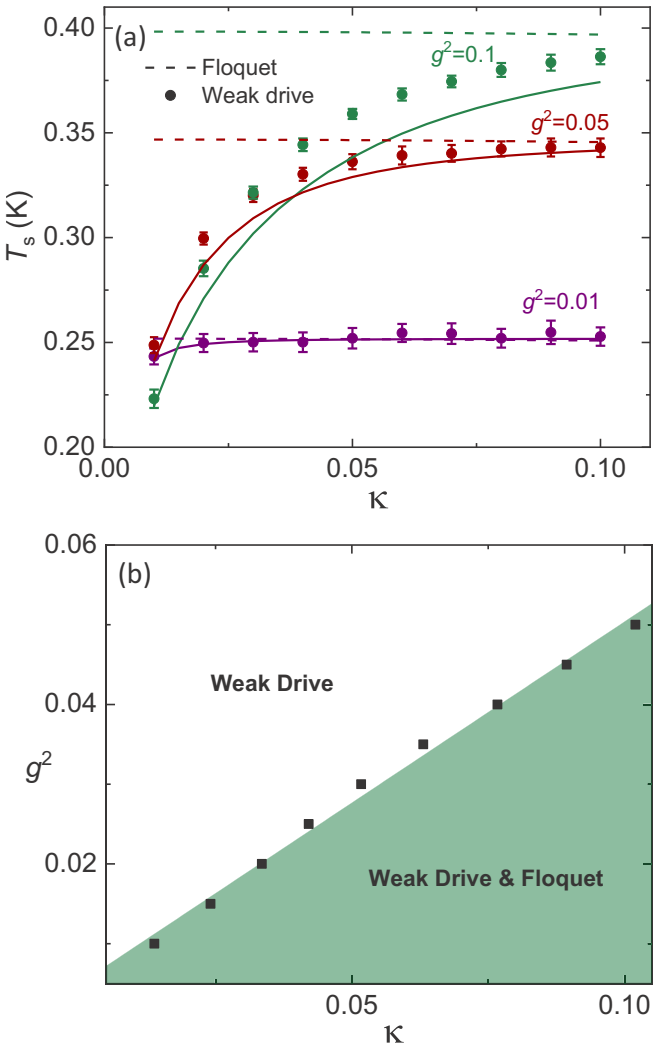

FIG. 3. A comparison of the stationary temperature T_S of the calorimeter for the weak-drive and Floquet modeling of the qubit dynamics obtained from numerics and analytics, (37) and [9], respectively. (a) Dependence of the stationary temperature on the driving strength κ for coupling g held constant. The dots are obtained numerically from the weak drive and the full line from the analytics. The striped lines are analytic results of the Floquet modeling. (b) Parametric region for which the Floquet-modeling T_S predictions correspond with the weak-drive-modeling predictions. In the green region, both predict the same values; in the white region only, they differ. The parameters used for the simulations are in the caption of Fig. 1.

equation (18). The quantum discord related to temperature measurements of qubit-temperature states as defined in (17) is zero. This tells us that although the hybrid master equation does not have a classical form, temperature measurements cannot detect any quantum effects.

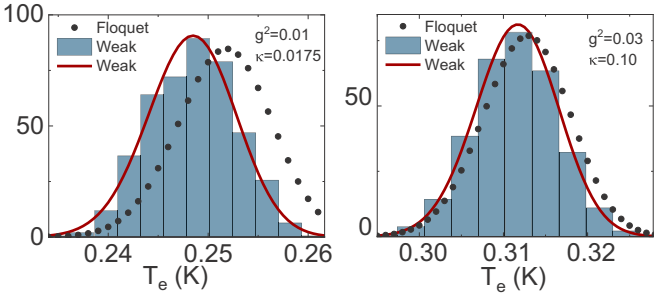

FIG. 4. Steady-state distribution obtained from the numerics (blue histogram) compared to the steady state predicted by the Fokker-Planck equation for the weak drive (37) (red line) and the Floquet Fokker-Planck equation (black circles) [9]. The parameters for the left distribution are outside of the region of validity for the Floquet; see Fig. 3(b). The parameters of the right figure are inside of this region.

Using multitimescale perturbation theory, we were able to reduce the full qubit-temperature process to an effective Fokker-Planck equation for the electron temperature (37).

We compared the numerical and analytic results for the weak-drive modeling of the qubit dynamics with the Floquet modeling studied in [9]. When the qubit-calorimeter coupling squared g^2 is small enough compared to κ, temperature predictions from both correspond well quantitatively. For a few periods of driving, they show the same temperature distributions. For long periods of driving, both modelings predict similar steady-state statistics. When the qubit-calorimeter coupling is increased such that the assumptions required for the Floquet approach are violated, the predictions of the models become quantitatively different. The Floquet modeling overestimates the power exerted from the qubit to the calorimeter. This can be explained by the observation that in the derivation of the Floquet stochastic jump equation, it is assumed that the driving strength is much larger than the qubit-calorimeter coupling squared. Using the steady-state temperature as an indicator, we estimated the regime of validity of the Floquet modeling of the qubit dynamics. The physical parameters under consideration are attainable in the experimental setup of [7], so that the regime of validity can be directly measured.

ACKNOWLEDGMENTS

We acknowledge the computational resources provided by the Aalto Science-IT project. The work of B.D. is supported by DOMAST. B.D. and P.M-G. also acknowledge support by the Centre of Excellence in Analysis and Dynamics of the Academy of Finland. The work of J.P.P. is funded through Academy of Finland Grant No. 312057 and from the European Union's Horizon 2020 research and innovation programme under the European Research Council (ERC) programme (Grant Agreement No. 742559).

APPENDIX A: BOUNDARY CONDITIONS

For Eqs. (4) and (13), we impose reflective boundary conditions at $X = 0$. We derive the master equation for the probability: let $f(\psi, \psi^*, X)$ be a smooth function; the time derivative of its average is

$$\frac{d}{dt}\mathsf{E}(f) = \int_0^{+\infty} dX \int D\psi D\psi^* \Big\{ \mathcal{L}^\dagger(f)(\psi, \psi^*, X)P(\psi, \psi^*, X) + K(\psi)\partial_\psi(f)(\psi, \psi^*, X)P(\psi, \psi^*, X) + K^*(\psi)\partial_{\psi^*}(f)(\psi, \psi^*, X)P(\psi, \psi^*, X) + \left[f\left(\phi_+, \bar{\phi}_+, X - \frac{\hbar\omega}{N\gamma}\right) - f(\psi, \psi^*, X)\right] G_\uparrow(X)\|\sigma_+\psi\|^2 P(\psi, \psi^*, X, t) + \left[f\left(\phi_-, \bar{\phi}_-, X + \frac{\hbar\omega}{N\gamma}\right) - f(\psi, \psi^*, X)\right] G_\downarrow(X)\|\sigma_-\psi\|^2 P(\psi, \psi^*, X, t)\Big\}, \tag{A1}$$

with $\phi_\pm$ the energy eigenstates of σ_z with eigenvalues ± 1, $G_{\uparrow/\downarrow}$ defined in (23), and

$$K(\psi) = -iH_q(t)\psi\, dt - \tfrac{1}{2}[G_\downarrow(X)(\sigma_+\sigma_- - \|\sigma_-\psi\|^2)\psi + G_\uparrow(X)(\sigma_-\sigma_+ - \|\sigma_+\psi\|^2)\psi] \tag{A2}$$

the continuous part of the stochastic differential equation for the qubit (4). After partial integration, Eq. (A1) becomes

$$\frac{d}{dt}\mathsf{E}(f) = \int_0^{+\infty} dX \int D\psi D\psi^* f(\psi, \psi^*, X)\{\mathcal{L}(P)(\psi, \psi^*, X) + \partial_\psi[K(\psi)P](\psi, \psi^*, X) + \partial_{\psi^*}[K^*(\psi)P](\psi, \psi^*, X)\} + \int_0^{+\infty} dX \int D\psi D\psi^* f(\psi, \psi^*, X) \int_0^{+\infty} dX' \int D\bar{\psi} D\bar{\psi}^* [W(\psi, X|\bar{\psi}, X')P(\bar{\psi}, \bar{\psi}^*, X', t) - W(\bar{\psi}, X'|\psi, X)P(\psi, \psi^*, X, t)] + \text{boundary terms}, \tag{A3}$$

with

$$W(\psi, X|\psi', X') = G_\uparrow(X')\|\sigma_+\psi'\|^2\delta\left(\frac{\sigma_+\psi'}{\|\sigma_+\psi'\|^2} - \psi\right)\delta(X' - \hbar\omega/\gamma - X) + G_\downarrow(X')\|\sigma_-\psi'\|^2\delta\left(\frac{\sigma_-\psi'}{\|\sigma_-\psi'\|^2} - \psi\right)\delta(X' + \hbar\omega/\gamma - X) \tag{A4}$$

and

boundary terms

$$= \frac{\Sigma V}{N\gamma}(T_p^5 - X^{5/2})Pf|_0^{+\infty} - \frac{10\Sigma V T_p^6}{2N\gamma} f\partial_X P\Big|_0^{+\infty} + \frac{10\Sigma V T_p^6}{2N\gamma} P\partial_X f\Big|_0^{+\infty} + \int D\psi D\psi^* \int_0^{\frac{\hbar\omega}{N\gamma}} dX \Big[f(\phi_+, \phi_+^*, -X)\|\sigma_+\psi\|^2 \times G_\uparrow\left(\frac{\hbar\omega}{N\gamma} - X\right) P\left(\psi, \psi^*, \frac{\hbar\omega}{N\gamma} - X\right) - f(\phi_-, \phi_-^*, X)\|\sigma_-\psi\|^2 G_\downarrow\left(X - \frac{\hbar\omega}{N\gamma}\right) P\left(\psi, \psi^*, X - \frac{\hbar\omega}{N\gamma}\right)\Big]. \tag{A5}$$

At infinity, the first three boundary terms drop since we assume that the probability and its derivative are zero at infinity. At $X = 0$, the first two terms cancel each other out due to the probability current being zero at the reflective boundary. The third term is zero as well; due to reflective boundary conditions, we consider functions which have zero derivative at $X = 0$. The first term in the integral is zero due to the θ function and the second term in the integral is zero since $P(\psi, \psi^*, X < 0) = 0$.

APPENDIX B: HYBRID MASTER EQUATION

Let us define the function

$$f(\psi, \psi^*, \xi) = \psi\, \psi^* \delta(\xi - X). \tag{B1}$$

Taking the average $\mathsf{E}(\cdot)$ of this equation gives the density operator as defined in Eq. (17),

$$\mathsf{E}[f(\psi, \psi^*, \xi)] = \rho(X, t). \tag{B2}$$

The differential of f is

$$df(\psi, \psi^*, \xi) = f(\psi + d\psi, \psi^* + d\psi^*, \xi + d\xi) - f(\psi, \psi^*, \xi) = \sum_{\substack{p=1 \\ p=k_1+k_2+k_3}}^{\infty} \frac{(d\xi)^{k_1}(d\psi^*)^{k_2}(d\psi)^{k_3}}{k_1!k_2!k_3!} \partial_\xi^{k_1}\partial_{\psi^*}^{k_2}\partial_\psi^{k_3} f(\psi, \psi^*, \xi). \tag{B3}$$

To proceed with the calculation, we use the explicit expressions (4) and (13) of the differentials. We simplify the above equation by making use of the rules of stochastic calculus; see, e.g., [30]. From stochastic calculus, it follows that $dw^2(t) = dt$,

$dw(t)\,dN_i = 0$, and $dN_i\,dN_j = \delta_{i,j}\,dN_i$. We thus get the Itô-Poisson stochastic differential,

$$df(\psi,\psi^*,\xi) = \left(\mathcal{L}_\xi^{(1)}\right)^\dagger f(\psi,\psi^*,\xi)\,dt + \left(\mathcal{L}_\xi^{(2)}\right)^\dagger f(\psi,\psi^*,\xi)\,dt + \frac{\sqrt{10\Sigma V k_B T_p^3}}{\gamma}\partial_\xi f(\psi,\psi^*,\xi)\,dw(t)$$
$$-\frac{i}{\hbar}[K(\psi)\partial_\psi - K(\psi)\partial_{\psi^*}]f(\psi,\psi^*,\xi)\,dt + \left[f\left(\phi_+,\phi_+^*,\xi-\frac{\hbar\omega}{N\gamma}\right) - f(\psi,\psi^*,\xi)\right]dN_\uparrow$$
$$+\left[f\left(\phi_-,\phi_-^*,\xi+\frac{\hbar\omega}{N\gamma}\right) - f(\psi,\psi^*,\xi)\right]dN_\downarrow, \tag{B4}$$

where $\phi_\pm$ are the eigenstates of σ_z, and $K(\psi)$ (A2) is the continuous part of the qubit stochastic differential equation (4). Taking the average $\mathsf{E}(\cdot)$ of Eq. (B4), we can simplify the equation. The term proportional to $dw(t)$ cancels due to the Itô description [30]. Using the definition of f (B1) gives the identity

$$\mathsf{E}\left[\psi\psi^*\left(\mathcal{L}_X^{(i)}\right)^\dagger\delta(\xi - X)\right] = \mathcal{L}_X^{(i)}\rho(X,t), \tag{B5}$$

for $i = 1,\ 2$. The average of the third line in Eq. (B4) gives

$$-\frac{i}{\hbar}[H(t),\rho(X,t)] + \frac{1}{2}\mathsf{E}\{[G_\downarrow(X)\|\sigma_-\psi\| + G_\uparrow(X)\|\sigma_+\psi\|]\psi\ \psi^*|\psi\} - \frac{1}{2}\{G_\downarrow(X)[\sigma_+\sigma_-,\rho(X,t)] + G_\uparrow(X)[\sigma_-\sigma_+,\rho(X,t)]\}. \tag{B6}$$

The last two lines become

$$G_\downarrow(X)\sigma_-\rho(X,t)\sigma_+ + G_\uparrow(X)\sigma_+\rho(X,t)\sigma_- - \tfrac{1}{2}\mathsf{E}\{[G_\downarrow(X)\|\sigma_-\psi\| + G_\uparrow(X)\|\sigma_+\psi\|]\psi\ \psi^*|\psi\}. \tag{B7}$$

Summing Eqs. (B5), (B6), and (B7) gives (18).

Discrete hybrid equation

The master equation (18) is a hybrid master equation. It describes the joint evolution of a classical variable, the temperature of the calorimeter squared $X = T_e^2$, and a quantum variable, the wave function of the qubit. The master equation (18) can be identified as the hybrid master equation proposed by [18].

First let us write the drift-diffusion terms from Eq. (18) as a discrete jump process,

$$\frac{d\rho}{dX}(X,t) = \sum_{j=\pm} G_j(X - j\Delta X)\rho(X - j\Delta X) - G_j(X)\rho(X) - \frac{i}{\hbar}[H(t),\rho(X)] + G_\downarrow\left(X-\frac{\hbar\omega}{N\gamma}\right)\sigma_-\rho\left(X-\frac{\hbar\omega}{N\gamma}\right)\sigma_+$$
$$+ G_\uparrow\left(X+\frac{\hbar\omega}{N\gamma}\right)\sigma_+\rho\left(X+\frac{\hbar\omega}{N\gamma}\right)\sigma_- - \frac{1}{2}G_\downarrow(X)\{\sigma_+\sigma_-,\rho(X)\} - \frac{1}{2}G_\uparrow(X)\{\sigma_-\sigma_+,\rho(X)\}, \tag{B8}$$

such that by taking the limit $\Delta X \to 0$, we retrieve the drift-diffusion process of the temperature squared. For a set initial temperature, the temperature is thus a discrete variable.

Let us now treat the temperature as a full quantum variable. That is, we expand the Hilbert space of the qubit with an infinite-dimensional Hilbert space, which corresponds to the discrete set of temperatures the calorimeter can reach according to Eq. (B8). Additionally, we define $e_{X,Y}$ as the projector from temperature-squared Y to X. We define the operator Φ acting on a qubit-temperature-squared operator a as

$$\Phi\,a = \sum_X \big[G_-(X)(e_{X+\Delta X,X}\otimes\mathbb{I})a(e_{X+\Delta X,X}^*\otimes\mathbb{I}) + G_+(X)(e_{X-\Delta X,X}\otimes\mathbb{I})a(e_{X-\Delta X,X}^*\otimes\mathbb{I})$$
$$+ G_\uparrow(X)\big(e_{X-\hbar\omega/N\gamma,X}\otimes\sigma_-\big)a\big(e_{X-\hbar\omega/N\gamma,X}^*\otimes\sigma_+\big) + G_\downarrow(X)\big(e_{X+\hbar\omega/N\gamma,X}\otimes\sigma_+\big)a\big(e_{X+\hbar\omega/N\gamma,X}^*\otimes\sigma_-\big)\big]. \tag{B9}$$

Following the results of [18], this operator is completely positive. Evolution with the adjoint Φ^* as the generator maps states diagonal in X onto states which are diagonal in X. A state which is diagonal in X evolves as

$$\rho(t) = \sum_X e_{X,X}\otimes\rho(X,t), \tag{B10}$$

where the qubit density at X $\rho(X,t)$ satisfies

$$\frac{d\rho(X,t)}{dt} = -\frac{i}{\hbar}[H(t),\rho(X,t)] + \sum_Y e_{X,Y}\Phi^*[\rho(t)]e_{X,Y}^* - \frac{1}{2}\sum_Y\{e_{Y,X}\Phi^*(\mathbb{I}),\rho(X,t)\}, \tag{B11}$$

which, in the limit of $\Delta X \downarrow 0$, gives (18).

APPENDIX C: EFFECTIVE TEMPERATURE EQUATION

We solve Eq. (31) at different orders by plugging in the Hilbert expansion (35). For physical parameters typical for the qubit-calorimeter experiment [7], the relevant temperature-(squared) range is much larger than $\hbar\omega/N\gamma$. For this reason, we will treat the rates $G_{\uparrow/\downarrow}(X)$ (23) as differentiable functions and ignore the small jump at $X = \hbar\omega/N\gamma$.

a. Order ε^0. The lowest-order equation is

$$M^{(0)}\vec{P}^0(X) = 0. \tag{C1}$$

The zeroth order of the Hilbert expansion (35) can be written into the form

$$\vec{P}(X,\tau) = F^{(0)}(X,\tau)\vec{Q}(X,\tau), \tag{C2}$$

where, taking $G(X) = G_\uparrow(X) + G_\downarrow(X)$,

$$\vec{Q}(X) = \frac{1}{G(X)^2 + 8\lambda^2}\begin{pmatrix} G_\uparrow(X)G(X) + 4\lambda^2 \\ G_\downarrow(X)G(X) + 4\lambda^2 \\ -2i\lambda[G_\downarrow(X) - G_\uparrow(X)] \\ 2i\lambda[G_\downarrow(X) - G_\uparrow(X)] \end{pmatrix} \tag{C3}$$

solves (C1) and satisfies $Q_1(X) + Q_2(X) = 1$.

b. Order ε^1. The first-order correction to $\vec{P}(X,t)$ solves

$$(M^{(0)}\vec{P}^{(1)})(X,\tau) = \frac{d\vec{P}^{(0)}}{d\tau}(X,\tau) - \left(\mathcal{L}_X^{(1)}\vec{P}^{(0)}\right)(X,\tau) - \partial_X(M^{(1)}\vec{P}^{(0)})(X,\tau). \tag{C4}$$

By Fredholm's alternative [29], the above equation is solvable if the solvability condition is satisfied. The solvability condition requires that the nonhomogeneous part of the above equation, i.e., the right-hand side, is zero on the kernel of the adjoint of $M^{(0)}$. Concretely, given that the kernel of $(M^{(0)})^\dagger$ is

$$v_1 = (1,\ 1,\ 0,\ 0), \tag{C5}$$

the solvability condition requires that

$$\partial_t F^{(0)} = \mathcal{L}_X^{(1)}F^{(0)} + \langle v_1|\partial_X M^{(1)}(\vec{Q}F^{(0)})\rangle \tag{C6}$$

should be satisfied.

The matrix $M^{(0)}$ has eigenvalues 0, λ_1, λ_2, λ_3, with corresponding right eigenvectors Q, w_2, w_3, w_4 and left eigenvectors v_1, v_2, v_3 and v_4. The vector $v_2 = (0,0,1,1)$, and it is straightforward to see that $\langle v_2, Q\rangle = 0$ and $v_2 \in \ker(M_1^\dagger)$. Projecting v_2 on both sides of Eq. (C4) gives

$$\langle v_2, M^{(0)}P^{(1)}\rangle = \lambda_2\langle v_2, P^{(1)}\rangle = 0. \tag{C7}$$

For $j = 3,\ 4$, we have

$$\begin{aligned}\lambda_j\langle v_j, P^{(1)}\rangle &= -\langle v_j|(\partial_X\vec{Q})f(X)F^{(0)}\rangle + \langle v_j|\vec{Q}\rangle\langle v_1|\partial_X(M^{(1)}F^{(0)})\rangle \\ &\quad - \langle v_j|\partial_X(M^{(1)}\vec{Q}F^{(0)})\rangle \\ &= -\langle v_j|(\partial_X\vec{Q})f(X)F^{(0)}\rangle - \langle v_j|\partial_X(M^{(1)}\vec{Q}F^{(0)})\rangle. \end{aligned}\tag{C8}$$

Going to the last line, we used that $\langle v_j, \vec{Q}\rangle = 0$ for $j \neq 1$ and $f(X) = -\frac{\Sigma V}{N\gamma}(T_p^5 - X^{5/2})$. Furthermore, the eigenvectors satisfy the completeness relation

$$\mathbb{I} = |Q\rangle\langle v_1| + \frac{|w_2\rangle\langle v_2|}{\langle v_2|w_2\rangle} + \frac{|w_3\rangle\langle v_3|}{\langle v_3|w_3\rangle} + \frac{|w_4\rangle\langle v_4|}{\langle v_4|w_4\rangle}. \tag{C9}$$

c. Order ε^2. We get the equation

$$\begin{aligned}&(M^{(0)}\vec{P}^{(2)})(X,\tau) \\ &= \frac{d\vec{P}^{(1)}}{d\tau}(X,\tau) - \left(\mathcal{L}_X^{(1)}\vec{P}^{(1)}\right)(X,\tau) \\ &\quad - \left(\mathcal{L}_X^{(2)}\vec{P}^{(0)}\right)(X,\tau) - (M^{(0)}\vec{P}^{(1)})(X,\tau) \\ &\quad - \partial_X(M^{(1)}\vec{P}^{(1)})(X,\tau) - \frac{1}{2}\partial_X(M^{(2)}\vec{P}^{(0)})(X,\tau). \end{aligned}\tag{C10}$$

By projecting the kernel of $(M^{(0)})^\dagger$ on (C10), we find the second-order solvability condition,

$$\begin{aligned}\partial_t F^{(1)} &= \mathcal{L}^{(1)}F^{(1)} + \mathcal{L}^{(2)}F^{(2)} + \langle v_1|\partial_X M^{(1)}P^{(1)}\rangle \\ &\quad + \left\langle v_1\middle|\partial_X^2 M^{(2)}P^{(0)}\right\rangle/2. \end{aligned}\tag{C11}$$

Using the completeness relation (C9) in the third term on the right-hand side, we find

$$\begin{aligned}&\partial_t F^{(1)} \\ &= \mathcal{L}^{(1)}F_1 + \mathcal{L}^{(2)}F_0 \\ &\quad + \langle v_1|\partial_X(M^{(1)}QF^{(1)})\rangle + \langle v_1|\partial_X\left(\frac{|(M^{(1)}w_3\rangle\langle v_3|P^{(1)}\rangle}{\langle v_3|w_\rangle}\right) \\ &\quad + \langle v_1|\partial_X\left(\frac{|(M^{(1)}w_4\rangle\langle v_4|P^{(1)}\rangle}{\langle v_4|w_4\rangle}\right) + \left\langle v_1\middle|\partial_X^2(M^{(2)}P^{(0)})\right\rangle/2. \end{aligned}\tag{C12}$$

By summing Eqs. (C6) and (C12), and using (C7) and (C8), we find the Fokker-Planck equation (37) for $F = F^{(0)} + \varepsilon F^{(1)}$.

[1] H. S. Leff and A. F. Rex, *Maxwell's Demon* (IOP, Philadelphia, 2003).

[2] J. V. Koski, V. F. Maisi, J. P. Pekola, and D. V. Averin, Proc. Natl. Acad. Sci. **111**, 13786 (2014).

[3] E. Aurell, K. Gawedzki, C. Mejía-Monasterio, R. Mohayaee, and P. Muratore-Ginanneschi, J. Stat. Phys. **147**, 487 (2012).

[4] P. Muratore-Ginanneschi and K. Schwieger, Phys. Rev. E **90**, 060102(R) (2014).

[5] B. Karimi and J. P. Pekola, Phys. Rev. Appl. **10**, 054048 (2018).

[6] J. Govenius, R. E. Lake, K. Y. Tan, and M. Möttönen, Phys. Rev. Lett. **117**, 030802 (2016).

[7] J. P. Pekola, P. Solinas, A. Shnirman, and D. V. Averin, New J. Phys. **15**, 115006 (2013).

[8] A. Kupiainen, P. Muratore-Ginanneschi, J. Pekola, and K. Schwieger, Phys. Rev. E **94**, 062127 (2016).

[9] B. Donvil, P. Muratore-Ginanneschi, J. P. Pekola, and K. Schwieger, Phys. Rev. A **97**, 052107 (2018).

[10] H. P. Breuer and F. Petruccione, Phys. Rev. A **55**, 3101 (1997).

[11] K. Szczygielski and R. Alicki, Phys. Rev. A **92**, 022349 (2015).

[12] K. Szczygielski, J. Math. Phys. **55**, 083506 (2014).

[13] R. Alicki, D. A. Lidar, and P. Zanardi, Phys. Rev. A **73**, 052311 (2006).

[14] G. Bulnes Cuetara, A. Engel, and M. Esposito, New J. Phys. **17**, 055002 (2015).
[15] H. P. Breuer and F. Petruccione, *The Theory of Open Quantum Systems* (Clarendon, Oxford, 2002).
[16] A. Rivas and S. F. Huelga, *Open Quantum System: An Introduction* (Springer, New York, 2012).
[17] J. Dalibard, Y. Castin, and K. Molmer, Phys. Rev. Lett. **68**, 580 (1992).
[18] D. Chruściński, A. Kossakowsi, G. Marmo, and E. C. G. Sudarshan, Open Syst. Inf. Dynam. **18**, 339 (2011).
[19] L. Diósi, Phys. Scr. **T163**, 014004 (2014).
[20] H. Ollivier and W. H. Zurek, Phys. Rev. Lett. **88**, 017901 (2001).
[21] H. Fröhlich, Proc. R. Soc. A **215**, 291 (1952).
[22] M. I. Kaganov, I. M. Lifshitz, and L. V. Tanatarov, J. Exptl. Theoret. Phys. (USSR) **31**, 232 (1956).
[23] F. C. Wellstood, C. Urbina, and J. Clarke, Phys. Rev. B **49**, 5942 (1994).
[24] J. P. Pekola and B. Karimi, J. Low Temp. Phys. **191**, 373 (2018).
[25] H. Pothier, S. Guéron, N. O. Birge, D. Esteve, and M. H. Devoret, Phys. Rev. Lett. **79**, 3490 (1997).
[26] S. Gasparinetti, K. L. Viisanen, O.-P. Saira, T. Faivre, M. Arzeo, M. Meschke, and J. P. Pekola, Phys. Rev. Appl. **3**, 014007 (2015).
[27] C. Wang, C. Axline, Y. Y. Gao, T. Brecht, Y. Chu, L. Frunzio, R. J. Devoret, and M. H. Schoelkopf, Appl. Phys. Lett. **107**, 162601 (2015).
[28] N. W. Ashcroft and N. D. Mermin, *Solid State Physics*, 1st ed. (Saunders College Publishing, Philadelphia, 1976).
[29] G. A. Pavliotis and A. M. Stuart, *Multiscale Methods: Averaging and Homogenization*, 1st ed. (Springer, New York, 2008).
[30] K. Jacobs, *Stochastic Processes for Physicists* (Cambridge University Press, Cambridge, 2010).